THE JOURNAL OF PHYSICAL CHEMISTRY B

Article

pubs.acs.org/JPCB

Membrane-Embedded Nanoparticles Induce Lipid Rearrangements Similar to Those Exhibited by Biological Membrane Proteins

Reid C. Van Lehn and Alfredo Alexander-Katz*

Department of Materials Science and Engineering, Massachusetts Institute of Technology, Cambridge, Massachusetts 02139, United States

Supporting Information

ABSTRACT: Amphiphilic monolayer-protected gold nanoparticles (NPs) have recently been shown to spontaneously fuse with lipid bilayers under typical physiological conditions. The final configuration of these NPs after fusion is proposed to be a bilayer-spanning configuration resembling transmembrane proteins. In this work, we use atomistic molecular dynamics simulations to explore the rearrangement of the surrounding lipid bilayer after NP insertion as a function of particle size and monolayer composition. All NPs studied induce local bilayer thinning and a commensurate decrease in local lipid tail order. Bilayer thickness changes of similar magnitude have been shown to drive protein aggregation, implying that NPs may also experience a membrane-mediated attraction. Unlike most membrane proteins, the exposed surface of the NP has a high charge density that causes electrostatic interactions to condense and reorient nearby lipid head groups. The decrease in tail order also leads to an increased likelihood of lipid tails spontaneously protruding toward solvent, a behavior related to the kinetic pathway for both NP insertion and vesicle−vesicle fusion. Finally, our results show that NPs can even extract lipids from the surrounding bilayer to preferentially intercalate within the exposed monolayer. These drastic lipid rearrangements are similar to the lipid mixing encouraged by fusion peptides, potentially allowing these NPs to be tuned to perform a similar biological function. This work complements previous studies on the NP−bilayer fusion mechanism by detailing the response of the bilayer to an embedded NP and suggests guidelines for the design of nanoparticles that induce controllable lipid rearrangements.

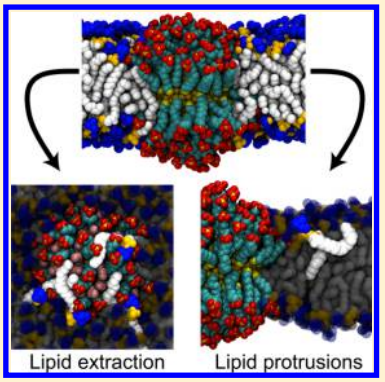

INTRODUCTION

Nanoparticles (NPs) are versatile materials with surface properties that can be tuned to mimic globular proteins in terms of size, chemistry, and solubility. In recent years, NPs have been increasingly used in biomedical applications including targeted drug delivery,[1,2] biosensing,[3,4] and bioimaging,[5] all applications that typically require contact between NPs and cell membranes. As a result, there is significant interest in engineering NPs for favorable interactions with the membrane while avoiding toxic side effects. A wealth of recent simulation and experimental studies using both cells and lipid bilayers, often used as a model for the full cell membrane, have shown that such nano−bio interactions depend strongly on the size and surface chemistry of the NPs.[6] For example, large NPs with diameters on the order of 10−100 nm that are able to adsorb to the bilayer surface, either due to specific ligand−receptor binding or nonspecific interactions, may be wrapped by the membrane and internalized via endocytosis.[7] The efficiency of wrapping has been shown to depend on the size of the NP, its shape, and its orientation.[8−11] A downside of this endocytic mechanism of cell entry, however, is that NPs may be trapped inside membrane-bound endosomal compartments and never access the cytosol.[12] In contrast, NPs smaller than 10 nm in diameter may insert into or translocate across the bilayer directly, although again with some limitations.[13−16] Purely hydrophobic NPs can stably embed within the hydrophobic bilayer core without inducing overt bilayer disruption, but they are insoluble in water.[17,18] Small cationic NPs can penetrate through the bilayer, but cell entry may involve the creation of membrane pores via a mechanism analogous to the pore formation caused by cationic peptides.[19−21] Such pore formation may lead to cytosolic leakage and eventual cell death, limiting the utility of cationic NPs in biomedical applications. There is thus ample interest in gaining physical insight into the behavior of NPs at cell interfaces in order to design NPs that can nondisruptively interact with cell membranes and ideally avoid cell uptake by endocytosis.

Recently, it was found that small (diameter <10 nm) anionic, amphiphilic, monolayer-protected gold NPs can nondisruptively fuse with lipid bilayers to obtain a transmembrane configuration reminiscent of membrane proteins.[22−26] The surface properties of these particles are determined by a protecting monolayer of largely hydrophobic alkanethiol ligands that are grafted to the gold core. A fraction of the ligands are end-functionalized with anionic sulfonate groups to confer aqueous solubility.[27] Using free energy calculations with an implicit bilayer model, we showed that this novel fusion process is driven by the hydrophobic effect as the alkane

Received: June 23, 2014
Revised: October 13, 2014
Published: October 15, 2014

   dx.doi.org/10.1021/jp506239p | J. Phys. Chem. B 2014, 118, 12586−12598

backbones shield exposed hydrophobic surface area in the core of the bilayer.[22,23,25,26] In order to reduce contact between the charged end groups and the hydrophobic bilayer core, the flexible alkanethiol backbones of the end-functionalized ligands deform to position the charged sulfonate groups at the aqueous interface. This process, called "snorkeling", has also been observed as a means of stabilizing charged transmembrane protein side chains.[28,29] The overall free energy change for NP insertion into the bilayer is largely a competition between the hydrophobic driving force and the free energy cost for end group snorkeling and as a result depends on the ratio of purely hydrophobic to end-functionalized ligands and the size of the NP.[22,23] Specifically, it was found that the free energy change for insertion is negative if the particle core diameter is smaller than a monolayer composition-dependent size threshold on the order of the thickness of the bilayer.[22,23] Molecular dynamics simulations also indicated that the kinetic pathway for fusion involves initial contact with hydrophobic lipid tails that protrude into solvent.[26] Finally, the NPs predicted to have the greatest fusion propensity in simulations were found to nondisruptively access the cell interior under conditions when endocytosis was blocked.[22,30] In sum, these studies show that the surface properties of the amphiphilic NPs are critical in determining the thermodynamic likelihood of fusion while bilayer fluctuations may affect fusion kinetics.

A major open question not addressed in the aforementioned research on NP−bilayer fusion is how NPs influence the surrounding bilayer after insertion. As membrane proteins may deform the bilayer, the physicochemial and structural similarity between embedded NPs and transmembrane proteins suggests that NPs may have similar effects. Previous studies of lipid rearrangements around transmembrane proteins have shown that proteins can modify the bilayer thickness, lipid tail disorder, lipid headgroup order, and other structural parameters.[31−33] Such perturbations of membrane structure can trigger protein aggregation,[34−36] cell signaling,[37,38] and membrane fusion.[39] It is possible that embedded NPs induce many of the same structural perturbations exhibited by proteins, but with the benefit of controllable surface properties. Furthermore, the lipid tail protrusions that mediate the initial insertion of NPs into the bilayer are rare events, but the frequency of such protrusions may increase in the vicinity of fusion peptides that disrupt the bilayer.[40,41] If embedded NPs can induce a similar increase in the tail protrusion likelihood, then it is possible that the presence of a single embedded NP may increase the likelihood of additional NP fusion. Identifying how embedded NPs influence the surrounding lipid annulus could thus provide insight useful to experimentalists and theorists alike who study similar NP systems.

In this work, we use atomistic molecular dynamics simulations to study lipid rearrangements around an embedded amphiphilic NP, complementing our previous studies of the thermodynamics and kinetics of the fusion pathway. In particular, we aim to identify how the choice of NP core diameter and monolayer composition affects changes in the surrounding lipid bilayer. The atomistic simulation methodology used here was chosen to accurately model the ligand fluctuations that remove charges from the bilayer core and stabilize the embedded state by effectively rearranging the NP surface properties.[13,22] The atomistic representation of the bilayer is superior to the implicit model used previously that lacks the molecular detail necessary to resolve lipid perturbations.[22,23,25] For example, the effective interface between the embedded NP and lipid membrane depends on the hydrophobic ligands, an effect not captured in implicit bilayer methods. The atomistic resolution is also valuable in studying lipid tail protrusions as coarse-grained models have shown large differences in the barrier to such protrusions relative to more detailed atomistic simulations.[40−43] Finally, the simulations also incorporate accurate long-range electrostatic effects to capture interactions between the highly charged NP surface and zwitterionic lipid head groups in detail. While several recent studies have used various coarse-grained or mean field models to study NP−bilayer interactions,[14−16,44−46] these approaches may be more appropriate for describing NPs with effectively static surface properties and lower surface charge densities where electrostatic effects may be less important. Mean field models also may lack the ability to capture the stochastic deformations of single lipids that atomistic models can resolve. Our simulations show that changing either the NP composition or NP core diameter has a significant effect on bilayer thinning near the NP−bilayer interface. We further find that the anionic NP surface attracts surrounding lipids due to their zwitterionic head groups, condensing lipids toward the NP surface and reorienting headgroup dipoles. Near the NP−bilayer interface, lipid tails are disordered and correspondingly lipid tail protrusions are enhanced as was previously observed in the vicinity of fusion peptides.[41] Finally, we find that lipids can be extracted from the bilayer entirely to preferentially adsorb onto the water-exposed NP monolayer. Our work shows that embedded NPs can drastically perturb the surrounding membrane with the extent of such deformation determined in part by the monolayer composition and particle size.

METHODS

Molecular dynamics simulations were conducted to simulate NPs embedded in a 1,2-dioleoyl-*sn*-glycero-3-phosphocholine (DOPC) bilayer in a physiological (150 mM) NaCl salt concentration at 300 K. DOPC was chosen as a typical membrane lipid that is in the fluid phase at room temperature and has a zwitterionic headgroup. All simulations used the GROMOS 54a7 united atom force field to model both the lipids and the NP.[47−49] The parametrization of the monolayer-protected NPs was recently described[47] and will only be briefly summarized here. The gold core of the NP was modeled as a hollow sphere with the mass of missing gold atoms redistributed uniformly to the shell. The sulfur atoms at the head of each grafted alkanethiol ligand were constrained to the NP shell and were not allowed to move on the NP surface. The SPC water model was used in accordance with the parametrization of GROMOS 54a7.[48] Additional details are in the Supporting Information.

To probe the role of monolayer composition and particle size in determining the deformation of the surrounding bilayer, several combinations of ligand compositions and particle sizes were simulated. Three ligand species were modeled: octanethiol (OT), heptadecanethiol (HDT), and 11-mercapto-1-undecanesulfonate (MUS). OT and HDT are purely hydrophobic with eight and 17 methylene groups respectively while MUS has an 11 methylene backbone and is end-functionalized with a sulfonate group that carries a single negative charge at physiological pH. The chemical structures of these three ligands are shown in Figure 1. Three different monolayer compositions were studied for particles with gold core diameters of both 2 and 3 nm, yielding a total of six simulation systems. The three compositions were all-MUS, 1:1 MUS:OT,

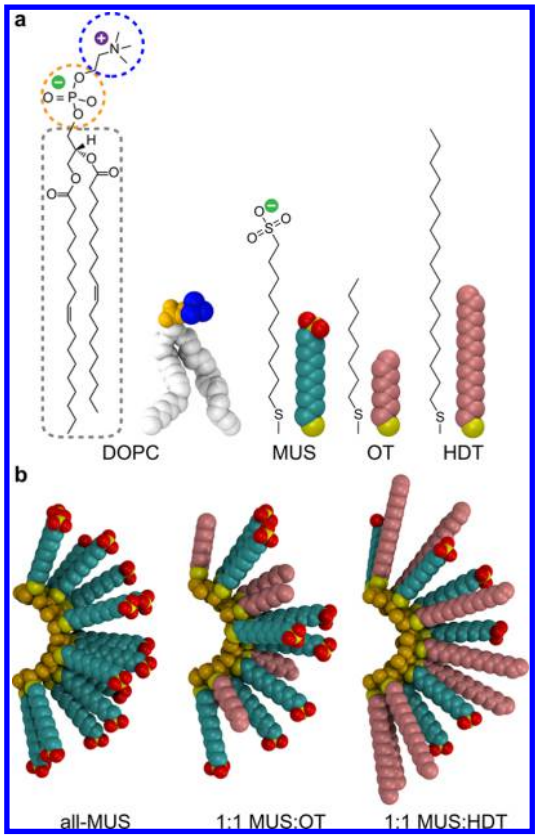

Figure 1. Illustration of different components in simulation systems. (a) Chemical structures and simulation representations of the lipid DOPC and the three ligand species. (b) Snapshots of 2 nm all-MUS, 1:1 MUS:OT, and 1:1 MUS:HDT NPs.

and 1:1 MUS:HDT. System components are summarized in Table S1.

Each NP was embedded in a lipid bilayer originally containing 512 DOPC molecules that had been pre-equilibrated for 100 ns in 150 mM salt solution. The size of the bilayer was chosen to ensure that any lipid deformations would decay before reaching the box edge. The NPs were embedded using the Gromacs program *g_membed*, a tool designed for the insertion of transmembrane proteins into the bilayer with minimal disruption.[50] Additional details on this procedure are in the Supporting Information (Figure S1).

Each NP–bilayer system was simulated for a total of 400 ns. The first 50 ns of each simulation were treated as equilibration time and were discarded during analysis. The 350 ns of sampling was sufficient to observe the convergence of structural measurements (see Figure S2 in the Supporting Information) as well as infrequent lipid extraction and tail protrusion events as will be described below. All six systems were simulated twice from different initial embedded positions and randomized initial velocities to provide better statistics for the system. A time step of 2 fs was used with a leapfrog molecular dynamics integrator. The temperature was set to 300 K using a velocity-rescale thermostat with a time constant of 0.1 ps. The pressure was maintained at 1 bar using a semiisotropic Parrinello–Rahman barostat with a time constant of 2.0 ps and a compressibility of 4.5×10^{-5} bar^{-1}. Electrostatic interactions were calculated using the smooth particle mesh Ewald summation method (PME) with a real space cutoff of 1.0 nm, a grid spacing of 0.12 nm, and fourth-order interpolation. The van der Waals and neighbor list cutoffs were similarly set to 1.0 nm following recent simulations of DOPC bilayers using PME and GROMOS 54a7.[49] Bond lengths were constrained using the LINCS algorithm.[51] All simulations were performed using Gromacs version 4.6.1.[52]

RESULTS AND DISCUSSION

General deformation profiles. The number densities of important system constituents were calculated around each embedded NP to illustrate the general deformation features. The NP–bilayer system was broadly divided into three components: the ligands that comprise the monolayer of the NP, the zwitterionic head groups of the DOPC lipids, and the hydrophobic lipid tails. Figure 2 plots the number densities of each of these components averaged radially around the axis of the NP, taking advantage of the cylindrical symmetry of the system in the plane of the bilayer (Figure S7). Accompanying the number density profiles are representative snapshots of each NP–bilayer system visualized according to the color scheme in Figure 1. For each plot, the vertical dashed line indicates the approximate interface between the NP and bilayer used for rescaling the radial axes in measurements reported below. The position of the NP–bilayer interface was defined as the distance radially away from the NP center where the average number density of sulfur atoms in the end groups of the MUS ligands is equivalent to the average number density of phosphorus atoms in the surrounding lipid head groups. More information on how this interface was determined and additional simulation snapshots are in the Supporting Information (Figures S3–S6).

Figure 2 illustrates several general features. From the NP ligand densities it is apparent that the choice of monolayer composition leads to different effective NP shapes. For the all-MUS particles, the snorkeling of all charged end groups into solvent leads to an hourglass-like shape that imposes a boundary on the tilt of nearby lipids. For MUS:OT particles, the hydrophobic ligands can fluctuate within the hydrophobic bilayer core, creating a more uniform, cylindrical interface. Finally, the longer ligands in the MUS:HDT monolayers preferentially extend out into the hydrophobic core, inverting the hourglass shape of the all-MUS particles to create a large barrel-like boundary. The difference in these boundary conditions has been proposed to lead to attraction for hourglass-like shapes and repulsion for barrel-like shapes,[53] so these profiles indicate that monolayer composition may affect membrane-mediated interactions between multiple embedded NPs or between NPs and transmembrane proteins.

For all NPs, the lipid headgroup densities show an apparent bilayer thinning effect in the vicinity of the NP as well as a slight enhancement of headgroup density near the NP–bilayer interface (slightly darker green in the color mapped density profile). The tail group densities further illustrate the thinning of the bilayer and generally match with the boundary conditions of the lipids. Another observation is a nonzero tail density in the region occupied by the NP for the 3 nm MUS:OT particle. Finally, comparing the 2 and 3 nm particle sizes show that the same basic features are observed for particles of the same composition, although the larger NPs lead to more pronounced deformations than the 2 nm particles (e.g., a thinner bilayer around the 3 nm all-MUS than 2 nm all-MUS particle). The origin of these different features will be discussed below.

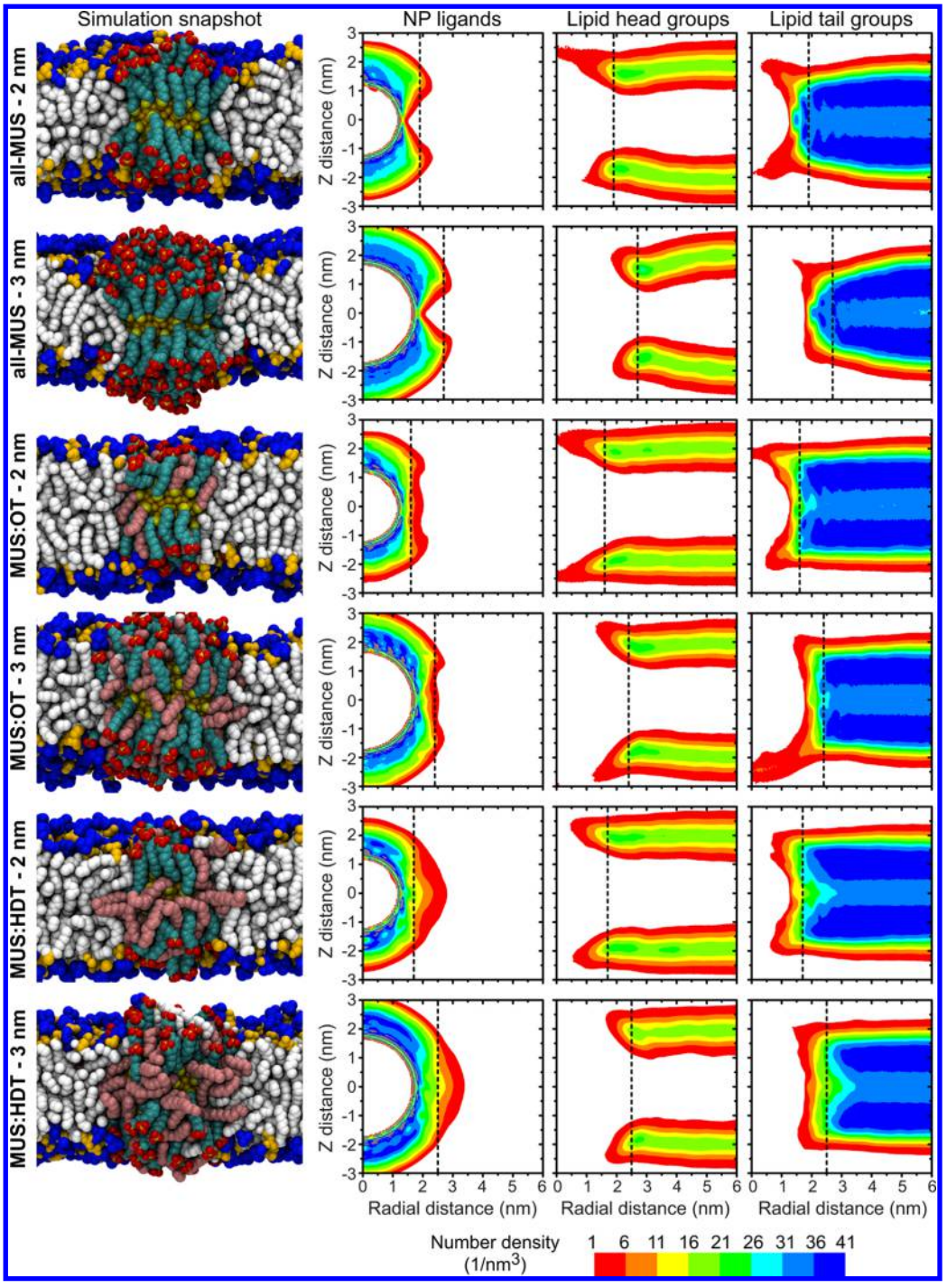

Figure 2. Number densities of various system components. Vertical dashed lines indicate the NP−bilayer interface as defined in the text. The snapshots follow the color scheme in Figure 1

All NPs induce negative hydrophobic mismatch. The number densities in Figure 2 show that all of the NPs studied give rise to local bilayer thinning, a result that was previously predicted using an implicit bilayer model[23,25] and agrees with a recent experimental study of NPs embedded in floating bilayers.[54] Figure 3 shows the radial thickness profiles of the bilayer around the 2 nm (a) and 3 nm (b) NPs. The bilayer thickness, D_{HH}, is calculated from the distance between the phosphorus atoms of the lipid head groups in the top and bottom monolayers as described in the Supporting Information. The MUS:HDT particles exhibit the lowest change in D_{HH} followed by MUS:OT and all-MUS, approximately following the amount of hydrophobic material present in the NP monolayer. A comparison between Figure 3a and 3b further shows that increasing the NP size causes additional thinning for all compositions. As the distance to the interface approaches 0, the bilayer thickness for all particle types increases with the MUS:OT and MUS:HDT particles inducing the largest increase. This thickness increase is because lipid head groups are electrostatically attracted to the MUS end groups while steric interactions with the hydrophobic ligands displace lipid tail groups from the bilayer center (Figure 2). Because the

dx.doi.org/10.1021/jp506239p | J. Phys. Chem. B 2014, 118, 12586−12598

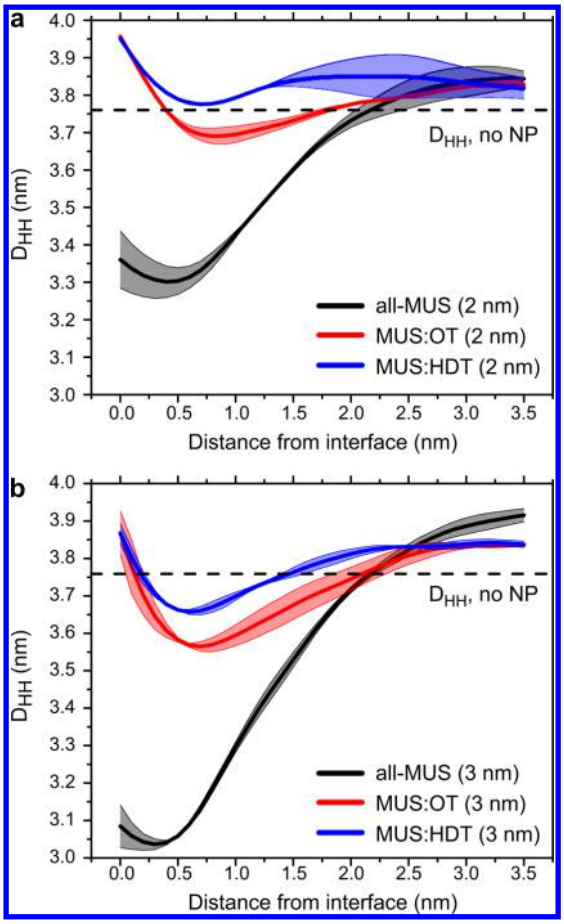

Figure 3. Thickness deformations around 2 nm core diameter NPs (a) and 3 nm core diameter NPs (b). The thickness is calculated as the distance between phosphorus atoms in opposite monolayers (D_{HH}) as detailed in the Supporting Information.

interfacial position is determined by the position of the MUS end groups, the hydrophobic ligands extend into the bilayer past the interface, leading to an increase for distances greater than 0. Finally, far from the NP the bilayer thickens relative to its thickness in the absence of the NP despite a plateau in D_{HH}. This effect is likely due to the increase in the sodium ion concentration when a NP is added with its counterions to the system; sodium ions bind with the choline head groups of DOPC leading to enhanced electrostatic repulsion between the two bilayer leaflets and increasing the bilayer thickness.[55]

The change in the bilayer thickness can be attributed to the principle of *hydrophobic matching* which refers to the local modulation of bilayer thickness to shield exposed hydrophobic material on transmembrane proteins from solvent.[31,56,57] The bilayer pays an energy cost for this disruption which is compensated by a reduction in the unfavorable solvation free energy of the hydrophobic surface in water. Local thickening and thinning of the bilayer are referred to as positive and negative mismatch conditions, respectively. For this system, the bilayer deforms to match the hydrophobic surface of the NP formed from the alkane backbones of the monolayer ligands. All NPs cause negative mismatch conditions with a thickness change of up to nearly 0.8 nm for the 3 nm all-MUS particle, an amount similar to what has been observed previously for deformations by transmembrane proteins.[31,57,58] As larger NPs induce greater thinning, similar degrees of mismatch may be possible for MUS:OT and MUS:HDT NPs with diameters larger than tested here.

Hydrophobic mismatch of this magnitude gives rise to a membrane-mediated attractive force based on minimizing the elastic deformation of the bilayer[53] that has been shown to drive protein aggregation in both simulations and experiments.[32,34−36,59] For example, multiple groups have used dissipative particle dynamic simulations of cylindrical proteins to show the formation of protein clusters for both positive and negative mismatch of less than 1 nm.[32,34] Similarly, coarse-grained molecular dynamics simulations using the MARTINI force field showed transmembrane protein clustering under conditions of ≈0.5 nm of negative mismatch[35] and revealed a ≈ 11 kcal/mol driving force for the dimerization of gramicidin A channels for ≈1.0 nm of negative mismatch.[33,60] Experimental approaches have also suggested protein aggregation under similar mismatch conditions. Monitoring the self-association of WALP peptides in bilayers of varying thicknesses showed an increase in aggregation for both positive and negative mismatch, agreeing with the previous simulation results.[59] Recent experiments of designed peptides reconstituted in unilamellar vesicles demonstrated protein oligomerization under negative mismatch conditions of approximately 0.9 nm in the presence of cholesterol.[36] The combination of particle-based simulations and experiments thus suggests that the negative mismatch induced by embedded NPs could lead to a membrane-mediated attractive interaction between NPs. The finding of a composition-dependent thickness profile implies that the magnitude of this driving force can be tuned by a choice of monolayer composition and particle size, potentially enabling tunable NP aggregation. However, the chief distinction between these NPs and typical proteins is the large charge density of the exposed monolayer, which may oppose aggregation due to electrostatic repulsion. Future work will focus on studying the dynamics of multiple embedded NPs to determine the balance of forces and whether aggregation is favorable.

Finally, it is interesting to note that bilayer thinning of approximately 1 nm, similar to the largest negative mismatch observed in Figure 3, was observed by Leroueil et al. in supported lipid bilayers near a variety of cationic nanoparticles and cell-penetrating peptides at low concentrations.[20] This thinning effect was hypothesized to precede lipid removal and hole formation and as a result is correlated with cytotoxic side effects.[20] However, such cationic nano-objects are believed to primarily adsorb to the surface of the membrane rather than embed within the bilayer like the NPs studied here.[20,61,62] Given that these anionic NPs can nondisruptively penetrate into cells[30] and can enter multilamellar vesicles without triggering dye leakage,[22] our findings indicate that the membrane thinning around embedded NPs is unlikely to induce pore formation despite the similar magnitude of the bilayer response in comparison to cationic nano-objects.

NPs condense head groups, reorient headgroup dipoles. In addition to thickness, another standard bilayer structural parameter is the area per lipid (APL), which is often used to indicate bilayer phase behavior. For example, lipid head groups in the gel phase assume a hexagonally close-packed configuration that reduces the APL substantially relative to lipids in the fluid phase.[63] Figure 4 shows the APL measured radially away from the NP−bilayer interface. The APL was measured by projecting the positions of the phosphorus atoms and all MUS end groups onto a plane and performing a

dx.doi.org/10.1021/jp506239p | J. Phys. Chem. B 2014, 118, 12586−12598

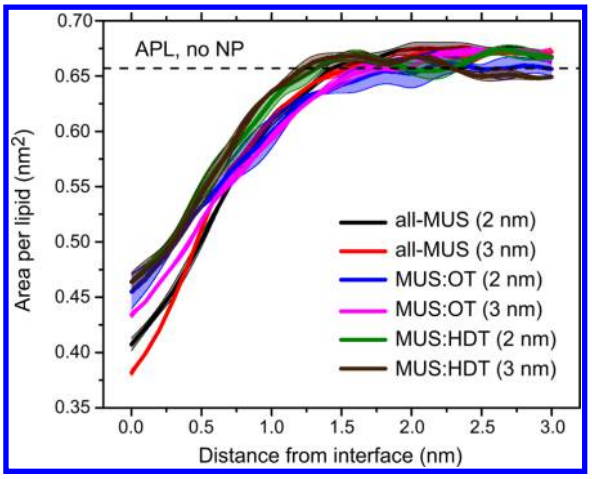

Figure 4. Area per lipid radially around all six NPs simulated. The dashed line indicates the APL for a pure bilayer with no NP as a control.

Voronoi tessellation to calculate the APL, then averaging the APL radially around the center of mass of the NP core. For all NPs, the APL decreases over approximately the same one nanometer length scale and with nearly the same magnitude independent of particle type, although the two all-MUS particles show the greatest decrease throughout the entire profile. At distances far from the NP−bilayer interface, the APL returns to its baseline value for a pure bilayer indicating no long-range disruption of lipid head groups.

This decrease in the APL may be interpreted as a general condensing effect - the lipids are dragged closer to the surface of the NP and correspondingly pack together at a greater density (lower APL). Interestingly, this condensing effect is achieved without thickening the bilayer, which is the response typical of gel phase lipids[63] or lipids condensed by cholesterol[64] in which lipid tails also straighten. The observation of a locally thinner bilayer despite the dense lipid headgroup packing implies that lipid tails are disordering, rather than ordering, as will be discussed below. The similarity of the APL profiles for all particle types suggests that the reason for lipid condensation is due to a shared property of all the particles. One possibility is that the high surface charge density of the NPs, a property not commonly associated with transmembrane proteins, attracts the zwitterionic DOPC head groups to the NP−bilayer interface. This electrostatic attraction would explain the decay of the APL over approximately 1.0 nm which is close to the Debye length of the system in 150 mM salt. The slightly lower APL for all-MUS particles may be due to their higher charge densities.

To test whether electrostatic effects play a role in the attraction of lipid head groups to the NP surface, the orientation of the $P^- \rightarrow N^+$ vector in the lipid head groups was calculated. The $P^- \rightarrow N^+$ dipole usually lies in the plane of the bilayer with no in-plane orientational preference, but in the presence of the charged NP it may rotate to bring the positively charged choline moieties closer to the negatively charged monolayer end groups. To quantify the extent of rotation, the angle θ was defined as the angle between the $P^- \rightarrow N^+$ vector and a vector drawn from the center of mass of the NP core to the phosphorus atom of the lipid, with both vectors projected into the $x-y$ plane as shown in Figure 5a. In a bilayer without an embedded NP the average value of cos θ was 0 as expected. In contrast, introducing any NP led to a decrease in cos θ as shown in Figure 5b. The decrease indicates a preferential

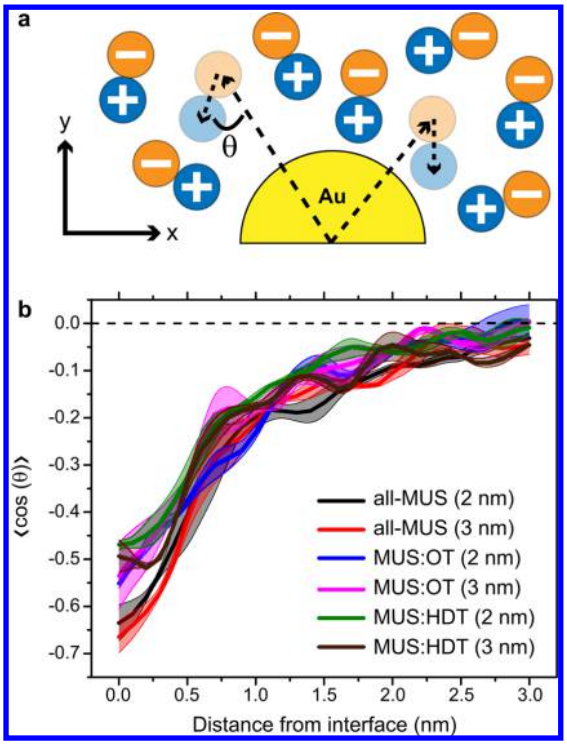

Figure 5. Reorientation of $P^- \rightarrow N^+$ dipoles near embedded NPs. (a) Definition of θ, the angle between the $P^- \rightarrow N^+$ vector and a reference vector to the NP center. (b) cos θ as a function of the radial distance of lipid heads from the NP−bilayer interface.

reorientation of choline groups to face the NP with a limiting value of −1 indicating complete rotation of all $P^- \rightarrow N^+$ to face toward the NP center.

As with the APL results, the change in the headgroup dipole orientation occurs mostly over the first nanometer from the NP−bilayer interface, with cos θ decreasing more slowly over the next two nanometers before achieving the bulk value. Head group reorientation can be attributed to electrostatic interactions so the observation of a similar length scale between this measurement and the APL measurements implies that both observations are related to electrostatic attraction, explaining why the same general trend is observed for all NPs. Similarly, both Figure 4 and Figure 5 show slightly more pronounced results for the higher charge density all-MUS particles. To the best of our knowledge, similar lipid headgroup reorientation has not been observed previously for lipid deformations around transmembrane proteins and the functional consequences of this effect are unknown.

NPs locally disorder lipid tails. Previous studies on negative hydrophobic mismatch conditions around transmembrane proteins have indicated that bilayer thinning should be accompanied by a decrease in tail order.[31] The change in tail order can be determined by calculating the deuterium order parameter, S_{CD}, for each of the methylene atoms in the lipid tails. The S_{CD} order parameter is defined as

$$S_{CD} = \frac{1}{2}\langle 3\cos^2\alpha - 1\rangle \quad (1)$$

where α is the angle between the $C \rightarrow D$ vector in a deuterated methlylene group and the bilayer normal. S_{CD} parameters are commonly compared to results from neutron scattering; larger values of S_{CD} are interpreted as indicating more tail order while lower values indicate disorder.[65] Here, the bilayer normal is

dx.doi.org/10.1021/jp506239p | J. Phys. Chem. B 2014, 118, 12586−12598

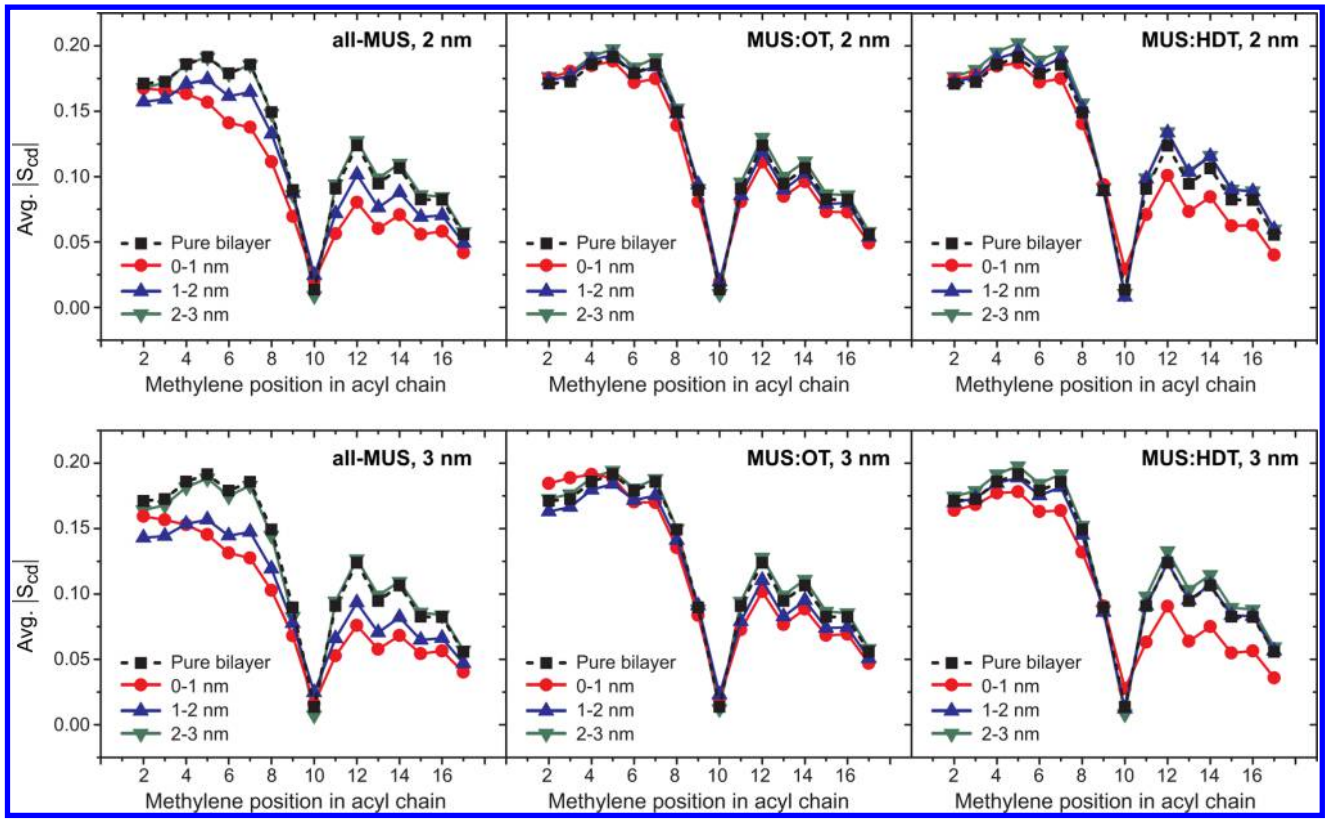

Figure 6. Lipid tail deuterium order parameters, S_{CD}, averaged over both the *sn*-1 and *sn*-2 tails. S_{CD} parameters are reported for each methylene position separately according to the scheme in Figure S8. Order parameters are reported separately for lipids 0−1 nm, 1−2 nm, and 2−3 nm away from the NP−bilayer interface. The order parameter for a pure bilayer with NP is shown as a black dashed line in each plot, though it is largely similar to the 2−3 nm results for all NPs.

assumed to be the *z*-axis and the $C \rightarrow D$ vectors are reconstructed geometrically.[66]

Figure 6 shows the S_{CD} profiles for each of the NPs, with separate profiles shown for lipids 0−1 nm, 1−2 nm, and 2−3 nm away from each NP. Methylene positions are numbered according to the scheme in Figure S8. The all-MUS particles show significant disordering for lipids up to 2 nm away, with the lipids 2−3 nm away showing similar S_{CD} profiles as a pure bilayer. The values for both 2 and 3 nm NPs are similar, implying that size is not as important as monolayer composition in determining tail group disorder. The MUS:OT particles only slightly decrease tail order for lipids up to 2 nm away while MUS:HDT particles decrease tail order for only the lipids within 0−1 nm of the NP−bilayer interface. Unlike the all-MUS particles, only the methylene groups near the end of the tails have decreased S_{CD} values for both the MUS:OT and MUS:HDT particles while the methylene positions closer to the headgroup are relatively unperturbed. The tail disorder results thus roughly follow the thickness profiles from Figure 3, with greater bilayer thinning corresponding to an enhanced decrease in lipid tail order. The shape of the NP boundary also likely contributes to the extent of disorder, as the cylindrical shape of the MUS:OT NP (Figure 2) is commensurate with the preferred cylindrical shape of DOPC lipids, while both the hourglass-like all-MUS NPs and barrel-like MUS:HDT NPs require a perturbation of the preferred lipid structure to accommodate their interfaces. This likely explains the more significant disordering for MUS:HDT for lipids 0−1 nm from the interface compared to MUS:OT despite a smaller thickness perturbation. Further analysis of the origin of the increased tail disorder shows that while the overall fraction of *gauche* dihedral angles is approximately unchanged near the NPs (Figure S8), there is a pronounced increase in the likelihood of consecutive *gauche* rotamers in the lipid tails that induces a large disruption of lipid packing consistent with the decrease in S_{CD} parameters (Figure S9). Similar second-order changes in dihedral sequences has been suggested to explain ordering effects by cholesterol in an analogous manner.[67] This finding confirms that the S_{CD} parameters are a suitable measure of tail disorder for this system.

Lipid tail protrusions enhanced in vicinity of NPs. In recent work, we showed that the apparent rate-limiting step for NP insertion into the embedded state studied here is the appearance of lipid tail protrusions.[26] Lipid tail protrusions in this context are defined as hydrophobic lipid tail atoms that stochastically protrude into the solvent-rich headgroup region of the bilayer where they may contact NPs near the bilayer surface and trigger insertion. While such protrusions are rare in planar bilayers, transmembrane fusion peptides may increase the probability of lipid tail protrusions in their vicinity by disrupting lipid tail order,[40,41] similar to the decrease in tail order observed in Figure 6. Based on this similarity, it is possible that lipid tail protrusions may also be more probable near embedded NPs.

A lipid was designated as protruding if any hydrophobic atom in its tail extended more than 0.1 nm into solvent beyond the nearest phosphorus atom as described in the Supporting Information. Previous work has shown that protrusions identified by this definition are associated with spontaneous vesicle fusion[40] and enhanced lipid mixing.[41] Two example

dx.doi.org/10.1021/jp506239p | J. Phys. Chem. B 2014, 118, 12586−12598

snapshots of spontaneous tail protrusions near embedded NPs are shown in Figure 7a. Figure 7b and 7c show the time-

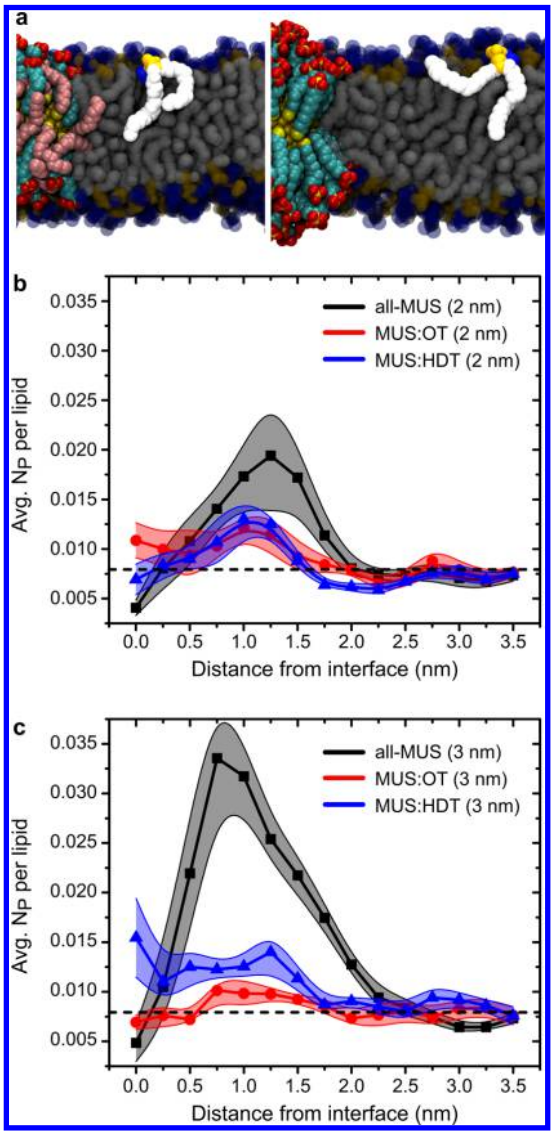

Figure 7. Analysis of lipid tail protrusions around embedded NPs. (a) Simulation snapshots showing an example of spontaneous protrusions (highlighted lipids) near a 2 nm MUS:HDT (left) and 3 nm all-MUS (right) NPs. (b) Average number of protruding lipids per lipid (N_p) near 2 nm NPs. (c) N_p for 3 nm NPs.

averaged number of protruding lipids, N_p, per lipid as a function of the radial distance from the NP−bilayer interface for 2 and 3 nm core diameter NPs, respectively. This measurement is effectively the probability of observing a protruding lipid in the vicinity of the NP. In both plots, the dashed horizontal line indicates the probability of observing a protruding lipid in a DOPC bilayer without an embedded NP. For both NP core diameters, there is an increase in protrusion probability in the vicinity (<2 nm) of all NPs, with the all-MUS NPs inducing the most significant increase. The 3 nm MUS:OT and MUS:HDT NPs have a slightly larger protrusion probability than the 2 nm NPs, while the 3 nm all-MUS NP clearly leads to the highest protrusion probability. These results agree well with the lipid tail disorder shown in Figure 6, where all-MUS NPs disrupted lipid tails to the greatest extent. Notably, peaks in the protrusion probability occur at approximately 1.0 nm from the interface for most of the NPs. This distance is roughly where the area per lipid begins to decrease from its typical value for DOPC (Figure 4). While Figure 6 indicates that tails become more disordered closer to the NP, the lower area per lipid indicates that head groups pack together more tightly within this region. As the lipid tails must pass through the headgroup region to access solvent, the tightly packed head groups likely act as a steric barrier to protrusions leading to the maximum enhancement in protrusion probability where the APL regains its unperturbed value while tails are still disordered. To confirm that these findings are not an artifact of the method for identifying protrusions, an alternative method for quantifying protrusions based on contact between hydrophobic tail atoms and water is presented in the Supporting Information (Figure S10) and shows similar trends.

The finding that an embedded NP increases the appearance of tail protrusions implies that the presence of an initial embedded NP may lower the barrier for the insertion of additional NPs in analogy with a nucleation-and-growth kinetic process. Moreover, the increased lipid tail disorder and increase in tail protrusion probability in the vicinity of the embedded NPs are also effects demonstrated by fusion peptides. In previous simulation studies, a single fusion peptide was shown to increase the probability of protrusions in its vicinity by a factor of about 4−6.[40,41] Here, the 3 nm all-MUS NP induces a ≈4.2× increase in protrusion probability at its peak position, commensurate with the fusion peptide results. While the other NPs only exhibit modest increases in protrusion probability, the increase in tail disorder with increasing NP size suggests that larger NPs may exhibit significantly higher protrusion probabilities. Based on our previous work, it is predicted that NPs of up to approximately 10 nm in core diameter can stably embed within membranes based on the choice of surface composition.[22,23] Given that the protrusion probability is correlated with increased tail disorder, it would be likely that these larger NPs would further enhance the likelihood of observing protrusions.

The appearance of lipid protrusions is also believed to be a critical step in the onset of vesicle−vesicle fusion. Previous simulation studies have shown that vesicle fusion proceeds in three stages with separate energy barriers - first, two vesicles approach until close contact between the bilayer occurs, then lipid tails begin to mix between the two apposed bilayers to form a metastable hemifusion intermediate, and finally the hemifused intermediate ruptures to form a fusion pore.[68,69] Several different simulation methodologies have shown that initial contact between lipid protrusions represents the barrier to lipid mixing.[40,42,43,70] Moreover, experimental measurements of fusion thermodynamics strongly support acyl chain protrusions as a likely first barrier in a three-stage fusion process.[71] Our findings thus suggest that embedded NPs reduce the barrier for the initial lipid mixing between two apposed bilayers. Moreover, electrostatic interactions with the zwitterionic lipid head groups also attract NPs to the surface of the bilayer.[26] Embedded NPs may also then mediate the approach of two vesicles to each other, reducing barriers for the first two stages of the fusion pathway described above in analogy to fusion peptides. The higher charge density of the all-MUS NPs, along with the higher protrusion probability in their vicinity, likely makes such NPs ideal for reducing both barriers. Future work will focus on this possibility as well as the influence that embedded NPs may have on the formation of a fusion pore.

dx.doi.org/10.1021/jp506239p | J. Phys. Chem. B 2014, 118, 12586−12598

Frequent lipid extraction facilitated by similarity between NP monolayer, bilayer. In Figure 2, the lipid tail density profile for the 3 nm MUS:OT particle shows a significant probability of finding lipid tails in a spatial region that overlaps with the density of NP ligands. This observation implies that lipids can be "extracted" from the bilayer entirely due to the chemical similarity between the hydrophobic lipid tails and the hydrophobic ligand backbones in the NP monolayer. Examination of the simulation trajectories led to the identification of transient lipid extraction events, in which lipids intercalated within the NP monolayer, for all of the simulations. Furthermore, it has recently been suggested in the literature that highly hydrophobic graphene sheets can extract lipids from intact bilayers in a similar process.[72] Our results suggest that such extraction events occur frequently near embedded NPs.

To explore the origin of this process, the Lennard-Jones interaction energies between a single extracted lipid and the NP, bilayer, and solvent were calculated during a 300 ns portion of a simulation run. The lipid was chosen from a 2 nm all-MUS simulation. The Lennard-Jones energies approximate van der Waals (nonpolar) forces between the hydrophobic lipid tails and ligand backbones. Figure 8a shows each of these energy components as well as their sum. The values are expressed as the change in the interaction energy relative to the average computed for the 100−110 ns time period. The dashed vertical lines mark the time when the lipid begins to move out of the bilayer and into the monolayer, indicating the onset of the extraction event, and the time when the lipid retracts back toward the bilayer, indicating the end of the extraction event, based on an order parameter described below. At the onset of extraction (≈160 ns), the LJ interaction energy between the lipid and the bilayer increases, but this energy increase is compensated by interactions with the NP. There is effectively no change in solvent interactions indicating that the lipid is shielded from water when intercalated within the monolayer. The sum of all three interaction energies shows an approximately constant value throughout the entire time frame indicating that lipid extraction occurs at constant energy and lipids near the NP−bilayer interface can be extracted to maximize their conformational freedom. Figure 8b shows top-down snapshots of the lipid transiently entering the monolayer as shown by the position of the lipid relative to the MUS end groups.

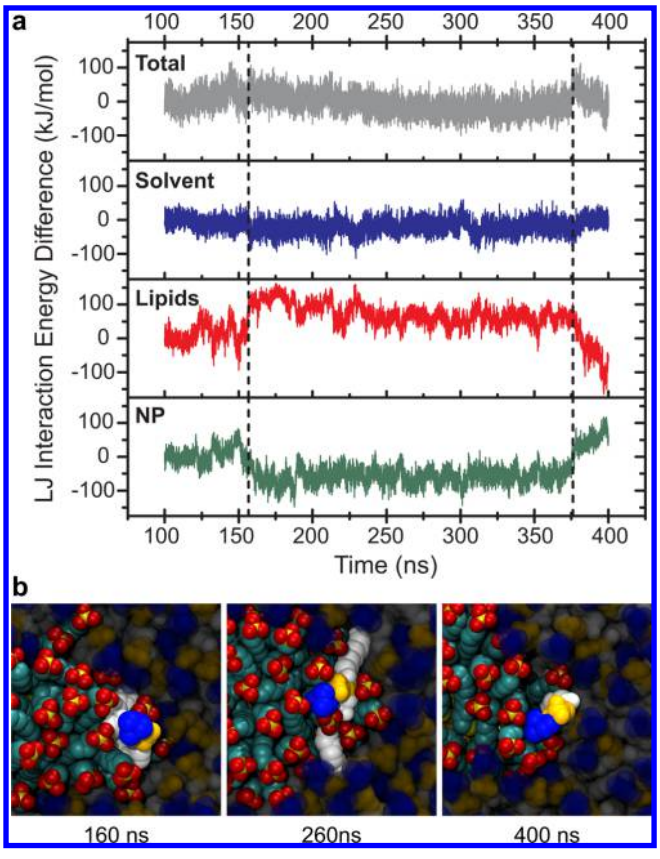

Figure 8. Energetics of transient lipid extraction. (a) Change in the Lennard-Jones interaction energy between the extracted lipid and system components as a function of time. The total change in energy is the sum of the solvent, lipid, and NP interactions. Dashed vertical lines indicate the start/end of extraction. (b) Top down snapshots of the extracted lipid and surrounding bilayer at the onset of extraction, 100 ns later, and after extraction.

To quantify the tendency of different NPs to extract lipids, a lipid tail atom was designated as extracted if no other hydrophobic lipid atoms were within 0.6 nm but at least four hydrophobic NP atoms were within the same distance. A lipid was then designated as extracted if at least four atoms in either tail met these criteria. This definition was able to accurately capture lipid extraction events based on the correlation between the vertical dashed lines in Figure 8 and the changes in lipid/NP interaction energies. Using this definition of lipid extraction, the number of extracted lipids per time was quantified for each NP composition. In general, lipid extraction was found to be common, with several lipids often being extracted concurrently. As an example, Figure 9 shows the number of extracted lipids as a function of time for a 3 nm MUS:OT NP and an example snapshot at 400 ns. The time plot illustrates that several lipids are consistently extracted simultaneously as is clearly observed in the simulation snapshot where four lipids have tails extending into the exposed NP monolayer. Figure S11 shows several more time plots and example snapshots for other monolayer compositions to emphasize that transient lipid extraction occurs frequently for all NPs studied.

Figure 9b shows the average number of lipids extracted per unit time for all NP types. For the 2 nm NPs, all three compositions showed similar tendencies to extract lipids within the error of the simulations. For 3 nm NPs, the more hydrophobic MUS:OT and MUS:HDT NPs were much more likely to extract lipids, while the all-MUS NP was even less likely to extract lipids than the 2 nm all-MUS NP. This difference is likely due to the reduced monolayer free volume in the larger all-MUS NP monolayer. For the MUS:OT and MUS:HDT particles, the removal of MUS ligands leads to a monolayer with both more free volume and more hydrophobicity, encouraging extraction significantly relative to the all-MUS NP. The 2 nm NPs likely demonstrate similar results due to a large amount of free volume for all compositions. Figure 9c plots the total number of unique lipids extracted over the 350 ns trajectories. This comparison shows that the MUS:HDT NPs extract more lipids than the other NPs which may be due to the tendency of the HDT lipids to extend into the bilayer core (c.f. Figure 2), excluding volume and forcing lipid tails toward the surface where they can more easily enter the NP monolayer. For all NPs, each extraction event lasted an average of 11.7 ns, with the longest observed extraction occurring for

dx.doi.org/10.1021/jp506239p | J. Phys. Chem. B 2014, 118, 12586−12598

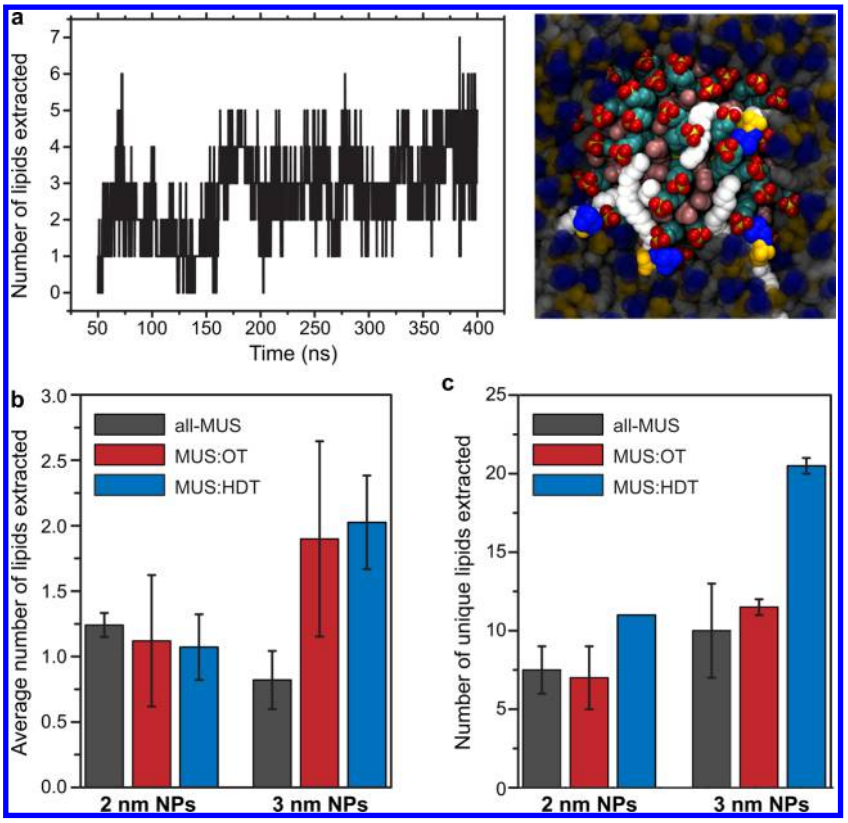

Figure 9. Effect of NP composition on lipid extraction. (a) Number of lipids extracted as a function of time for a 3 nm MUS:OT NP, with a single snapshot at 400 ns illustrating four lipids simultaneously extracted from a single monolayer. (b) Number of lipids extracted for all NPs, time-averaged over 350 ns for each NP. Error bars represent error between two separate simulation trajectories. (c) Number of unique lipids extracted for each NP composition over the total 350 ns trajectory.

287 ns. Table S2 summarizes the average time of an extraction event for each of the different NPs simulated as well as the longest extraction event recorded. No significant difference in the residence time of extracted lipieds was found for different NP types. Extraction events in excess of 100 ns were found for 9 of the 12 simulations, indicating that extraction can persist for long times independent of NP composition.

The transient lipid extraction events further illustrate the widespread bilayer disruption caused by embedded NPs. Moreover, it is unclear what consequences such extraction might have in a system with multiple vesicles or bilayers. Referring back to the three-stage pathway of vesicle−vesicle fusion discussed above, it is likely that these extraction events could facilitate the lipid mixing associated with the second stage of vesicle fusion if an embedded NP is in contact with a second vesicle. These results thus further support the idea that embedded NPs can act as biomimetic fusion peptides.

■ CONCLUSIONS

In this work, we used atomistic molecular dynamics simulations to gain insight into the effect of embedded NPs on the surrounding lipid bilayer. We specifically sought to understand how changing the size or monolayer composition of the NPs, two tuning parameters controllable synthetically, could influence the rearrangement of lipids. Our results show that all NPs simulated locally thin the bilayer, with the extent of thinning related to the monolayer composition. This negative hydrophobic mismatch has been previously shown to induce the clustering of proteins due to membrane-mediated interactions, and as a result there may be a driving force for NP aggregation as well. Due to the high charge density of the exposed monolayer, electrostatic interactions attract and reorient lipid head groups toward the NP, reducing the effective area per lipid in the vicinity of the NP−bilayer interface as well as causing a preferential reorientation of the headgroup dipoles. Despite this apparent ordering of lipid head groups, the lipid tail groups have decreased order due to the thinning of the bilayer. The combination of headgroup ordering and tail group disordering is unusual and to our knowledge has not been reported previously. The choice of monolayer composition and particle size is critical in determining both the extent of the thickness deformation and resulting decrease in tail group order. In future work, we will study how the combination of membrane-mediated attraction due to bilayer thinning and electrostatic repulsion affects the potential aggregation of multiple embedded NPs based on these findings.

In addition to these changes in basic structural features of the surrounding bilayer, our analysis also shows that embedded NPs can enhance the probability of lipid tails protruding toward solution and transiently extract lipids out of the bilayer and into the NP monolayer. As the initial insertion of the NPs into the embedded state depends on similar lipid protrusions, the increased protrusion propensity near embedded NPs suggests that cooperativity between NPs may assist insertion. Furthermore, the observation of both lipid extraction and enhanced protrusions suggests that novel interactions between embedded NPs and other lipid structures in solution, such as nearby micelles or vesicles, may be possible, including the possibility that NPs facilitate vesicle−vesicle fusion by assisting in lipid mixing between apposed vesicles. This work suggests

dx.doi.org/10.1021/jp506239p | J. Phys. Chem. B 2014, 118, 12586−12598

the intriguing possibility that these transmembrane NPs could be synthetic analogues to biological fusion peptides by both attracting nearby vesicles electrostatically and mediating the initial stages of membrane fusion, while having the benefit of being inserted into vesicles spontaneously in solution. Our results suggest that all-MUS NPs may be ideal for this purpose because of their high charge density and large increase in protrusion probability. Future work will focus on understanding how embedded NPs may mediate these processes by focusing on simulations between multiple membranes in the presence of embedded NPs. This work also suggests that cooperative interactions between NPs may occur, and thus additional work will elucidate the role of membrane rearrangement in reducing the barrier to NP insertion and mediating NP aggregation. This work thus shows several novel lipid rearrangements around embedded NPs and illustrates how the extent of deformation may be controlled by tuning the surface composition and size of the particle, potentially leading to design guidelines for novel nano−bio hybrid structures.

■ ASSOCIATED CONTENT

Supporting Information

Details of the NP model, embedding methodology, and simulation systems; methods for calculating simulation observables; additional discussion on tail order, lipid protrusions, and lipid extraction. This material is available free of charge via the Internet at http://pubs.acs.org.

■ AUTHOR INFORMATION

Corresponding Author

*E-mail: aalexand@mit.edu.

Notes

The authors declare no competing financial interest.

■ ACKNOWLEDGMENTS

R.C.V.L. was supported in part by a National Science Foundation Graduate Research Fellowship. R.C.V.L. and A.A.K. also acknowledge support by the MRSEC Program of the National Science Foundation under award number DMR-0819762. The simulations in this work used the Extreme Science and Engineering Discovery Environment (XSEDE), which is supported by National Science Foundation grant number OCI-1053575. Some of the computations in this paper were run on the Odyssey cluster supported by the FAS Sciences Division Research Computing Group.

■ REFERENCES

(1) Davis, M. E.; Chen, Z. G.; Shin, D. M. Nanoparticle Therapeutics: an Emerging Treatment Modality for Cancer. *Nat. Rev. Drug Discovery* **2008**, *7*, 771−782.

(2) Ghosh, P.; Han, G.; De, M.; Kim, C. K.; Rotello, V. M. Gold Nanoparticles in Delivery Applications. *Adv. Drug Delivery Rev.* **2008**, *60*, 1307−1315.

(3) Selvan, S. T.; Tan, T. T. Y.; Yi, D. K.; Jana, N. R. Functional and Multifunctional Nanoparticles for Bioimaging and Biosensing. *Langmuir* **2010**, *26*, 11631−11641.

(4) Jiang, S.; Win, K. Y.; Liu, S.; Teng, C. P.; Zheng, Y.; Han, M.-Y. Surface-Functionalized Nanoparticles for Biosensing and Imaging-Guided Therapeutics. *Nanoscale* **2013**, *5*, 3127−3148.

(5) Erathodiyil, N.; Ying, J. Y. Functionalization of Inorganic Nanoparticles for Bioimaging Applications. *Acc. Chem. Res.* **2011**, *44*, 925−935.

(6) Nel, A. E.; Mädler, L.; Velegol, D.; Xia, T.; Hoek, E. M. V.; Somasundaran, P.; Klaessig, F.; Castranova, V.; Thompson, M. Understanding Biophysicochemical Interactions at the Nano-Bio Interface. *Nat. Mater.* **2009**, *8*, 543−557.

(7) Bareford, L. M.; Swaan, P. W. Endocytic Mechanisms for Targeted Drug Delivery. *Adv. Drug Delivery Rev.* **2007**, *59*, 748−758.

(8) Chithrani, B. D.; Ghazani, A. A.; Chan, W. C. W. Determining the Size and Shape Dependence of Gold Nanoparticle Uptake into Mammalian Cells. *Nano Lett.* **2006**, *6*, 662−668.

(9) Huang, C.; Zhang, Y.; Yuan, H.; Gao, H.; Zhang, S. Role of Nanoparticle Geometry in Endocytosis: Laying Down to Stand Up. *Nano Lett.* **2013**, *13*, 4546−4550.

(10) Yi, X.; Shi, X.; Gao, H. A Universal Law for Cell Uptake of One-Dimensional Nanomaterials. *Nano Lett.* **2014**, *14*, 1049−1055.

(11) Dasgupta, S.; Auth, T.; Gompper, G. Shape and Orientation Matter for the Cellular Uptake of Nonspherical Particles. *Nano Lett.* **2014**, *14*, 687−693.

(12) Varkouhi, A. K.; Scholte, M.; Storm, G.; Haisma, H. J. Endosomal Escape Pathways for Delivery of Biologicals. *J. Controlled Release* **2011**, *151*, 220−228.

(13) Van Lehn, R. C.; Alexander-Katz, A. Penetration of Lipid Bilayers by Nanoparticles with Environmentally-Responsive Surfaces: Simulations and Theory. *Soft Matter* **2011**, *7*, 11392−11404.

(14) Li, Y.; Li, X.; Li, Z.; Gao, H. Surface-Structure-Regulated Penetration of Nanoparticles Across a Cell Membrane. *Nanoscale* **2012**, *4*, 3768−3775.

(15) Nangia, S.; Sureshkumar, R. Effects of Nanoparticle Charge and Shape Anisotropy on Translocation through Cell Membranes. *Langmuir* **2012**, *28*, 17666−17671.

(16) Gkeka, P.; Sarkisov, L.; Angelikopoulos, P. Homogeneous Hydrophobic−Hydrophilic Surface Patterns Enhance Permeation of Nanoparticles through Lipid Membranes. *J. Phys. Chem. Lett.* **2013**, *4*, 1907−1912.

(17) Wong-Ekkabut, J.; Baoukina, S.; Triampo, W.; Tang, I.-M.; Tieleman, D. P.; Monticelli, L. Computer Simulation Study of Fullerene Translocation Through Lipid Membranes. *Nat. Nanotechnol.* **2008**, *3*, 363−368.

(18) Rasch, M. R.; Rossinyol, E.; Hueso, J. L.; Goodfellow, B. W.; Arbiol, J.; Korgel, B. A. Hydrophobic Gold Nanoparticle Self-Assembly with Phosphatidylcholine Lipid: Membrane-Loaded and Janus Vesicles. *Nano Lett.* **2010**, *10*, 3733−3739.

(19) Shai, Y. Mechanism of the Binding, Insertion and Destabilization of Phospholipid Bilayer Membranes by Alpha-Helical Antimicrobial and Cell Non-Selective Membrane-Lytic Peptides. *Biochim. Biophys. Acta* **1999**, *1462*, 55−70.

(20) Leroueil, P. R.; Berry, S. A.; Duthie, K.; Han, G.; Rotello, V. M.; McNerny, D. Q.; Baker, J. R.; Orr, B. G.; Banaszak Holl, M. M. Wide Varieties of Cationic Nanoparticles Induce Defects in Supported Lipid Bilayers. *Nano Lett.* **2008**, *8*, 420−424.

(21) Chen, J.; Hessler, J. A.; Putchakayala, K.; Panama, B. K.; Khan, D. P.; Hong, S.; Mullen, D. G.; DiMaggio, S. C.; Som, A.; Tew, G. N.; et al. Cationic Nanoparticles Induce Nanoscale Disruption in Living Cell Plasma Membranes. *J. Phys. Chem. B* **2009**, *113*, 11179−11185.

(22) Van Lehn, R. C.; Atukorale, P. U.; Carney, R. P.; Yang, Y.-S.; Stellacci, F.; Irvine, D. J.; Alexander-Katz, A. Effect of Particle Diameter and Surface Composition on the Spontaneous Fusion of Monolayer-Protected Gold Nanoparticles with Lipid Bilayers. *Nano Lett.* **2013**, *13*, 4060−4067.

(23) Van Lehn, R. C.; Alexander-Katz, A. Free Energy Change for Insertion of Charged, Monolayer-Protected Nanoparticles into Lipid Bilayers. *Soft Matter* **2014**, *10*, 648−658.

(24) Carney, R. P.; Astier, Y.; Carney, T. M.; Voïtchovsky, K.; Jacob Silva, P. H.; Stellacci, F. Electrical Method to Quantify Nanoparticle Interaction with Lipid Bilayers. *ACS Nano* **2013**, *7*, 932−942.

(25) Van Lehn, R. C.; Alexander-Katz, A. Fusion of Ligand-Coated Nanoparticles with Lipid Bilayers: Effect of Ligand Flexibility. *J. Phys. Chem. A* **2014**, *118*, 5848−5856.

(26) Van Lehn, R. C.; Ricci, M.; Silva, P. H. J.; Andreozzi, P.; Reguera, J.; Voïtchovsky, K.; Stellacci, F.; Alexander-Katz, A. Lipid Tail Protrusions Mediate the Insertion of Nanoparticles into Model Cell Membranes. *Nat. Commun.* **2014**, *5*, 4482.

(27) Uzun, O.; Hu, Y.; Verma, A.; Chen, S.; Centrone, A.; Stellacci, F. Water-Soluble Amphiphilic Gold Nanoparticles With Structured Ligand Shells. *Chem. Commun.* **2008**, 196.
(28) Dorairaj, S.; Allen, T. W. On the Thermodynamic Stability of a Charged Arginine Side Chain in a Transmembrane Helix. *Proc. Natl. Acad. Sci. U.S.A.* **2007**, *104*, 4943−4948.
(29) Johansson, A. C. V.; Lindahl, E. Protein Contents in Biological Membranes Can Explain Abnormal Solvation of Charged and Polar Residues. *Proc. Natl. Acad. Sci. U.S.A.* **2009**, *106*, 15684−15689.
(30) Verma, A.; Uzun, O.; Hu, Y.; Hu, Y.; Han, H.-S.; Watson, N.; Chen, S.; Irvine, D. J.; Stellacci, F. Surface-Structure-Regulated Cell-Membrane Penetration by Monolayer-Protected Nanoparticles. *Nat. Mater.* **2008**, *7*, 588−595.
(31) Kandasamy, S.; Larson, R. Molecular Dynamics Simulations of Model Trans-Membrane Peptides in Lipid Bilayers: a Systematic Investigation of Hydrophobic Mismatch. *Biophys. J.* **2006**, *90*, 2326−2343.
(32) de Meyer, F. J.-M.; Venturoli, M.; Smit, B. Molecular Simulations of Lipid-Mediated Protein-Protein Interactions. *Biophys. J.* **2008**, *95*, 1851−1865.
(33) Yoo, J.; Cui, Q. Three-Dimensional Stress Field Around a Membrane Protein: Atomistic and Coarse-Grained Simulation Analysis of Gramicidin A. *Biophys. J.* **2013**, *104*, 117−127.
(34) Schmidt, U.; Guigas, G.; Weiss, M. Cluster Formation of Transmembrane Proteins Due to Hydrophobic Mismatching. *Phys. Rev. Lett.* **2008**, *101*, 128104.
(35) Parton, D. L.; Klingelhoefer, J. W.; Sansom, M. S. P. Aggregation of Model Membrane Proteins, Modulated by Hydrophobic Mismatch, Membrane Curvature, and Protein Class. *Biophys. J.* **2011**, *101*, 691−699.
(36) Kaiser, H.-J.; Orlowski, A.; Róg, T.; Nyholm, T. K. M.; Chai, W.; Feizi, T.; Lingwood, D.; Vattulainen, I.; Simons, K. Lateral Sorting in Model Membranes by Cholesterol-Mediated Hydrophobic Matching. *Proc. Natl. Acad. Sci. U.S.A.* **2011**, *108*, 16628−16633.
(37) Phillips, R.; Ursell, T.; Wiggins, P.; Sens, P. Emerging Roles for Lipids in Shaping Membrane-Protein Function. *Nature* **2009**, *459*, 379−385.
(38) Lundbaek, J. A.; Koeppe, R. E.; Andersen, O. S. Amphiphile Regulation of Ion Channel Function by Changes in the Bilayer Spring Constant. *Proc. Natl. Acad. Sci. U.S.A.* **2010**, *107*, 15427−15430.
(39) Kozlov, M. M.; McMahon, H. T.; Chernomordik, L. V. Protein-Driven Membrane Stresses in Fusion and Fission. *Trends Biochem. Sci.* **2010**, *35*, 699−706.
(40) Kasson, P. M.; Lindahl, E.; Pande, V. S. Atomic-Resolution Simulations Predict a Transition State for Vesicle Fusion Defined by Contact of a Few Lipid Tails. *PLoS Comput. Biol.* **2010**, *6*, e1000829.
(41) Larsson, P.; Kasson, P. M. Lipid Tail Protrusion in Simulations Predicts Fusogenic Activity of Influenza Fusion Peptide Mutants and Conformational Models. *PLoS Comput. Biol.* **2013**, *9*, e1002950.
(42) Mirjanian, D.; Dickey, A. N.; Hoh, J. H.; Woolf, T. B.; Stevens, M. J. Splaying of Aliphatic Tails Plays a Central Role in Barrier Crossing During Liposome Fusion. *J. Phys. Chem. B* **2010**, *114*, 11061−11068.
(43) Smirnova, Y. G.; Marrink, S.-J.; Lipowsky, R.; Knecht, V. Solvent-Exposed Tails as Prestalk Transition States for Membrane Fusion at Low Hydration. *J. Am. Chem. Soc.* **2010**, *132*, 6710−6718.
(44) Pogodin, S.; Baulin, V. A. Can a Carbon Nanotube Pierce Through a Phospholipid Bilayer? *ACS Nano* **2010**, *4*, 5293−5300.
(45) Pogodin, S.; Slater, N. K. H.; Baulin, V. A. Surface Patterning of Carbon Nanotubes Can Enhance Their Penetration Through a Phospholipid Bilayer. *ACS Nano* **2011**, *5*, 1141−1146.
(46) Ding, H.-M.; Tian, W.-d.; Ma, Y.-Q. Designing Nanoparticle Translocation Through Membranes by Computer Simulations. *ACS Nano* **2012**, *6*, 1230−1238.
(47) Van Lehn, R. C.; Alexander-Katz, A. Structure of Mixed-Monolayer-Protected Nanoparticles in Aqueous Salt Solution from Atomistic Molecular Dynamics Simulations. *J. Phys. Chem. C* **2013**, *117*, 20104−20115.
(48) Schmid, N.; Eichenberger, A. P.; Choutko, A.; Riniker, S.; Winger, M.; Mark, A. E.; van Gunsteren, W. F. Definition and Testing of the GROMOS Force-Field Versions 54A7 and 54B7. *Eur. Biophys. J.* **2011**, *40*, 843−856.
(49) Poger, D.; Mark, A. E. Lipid Bilayers: The Effect of Force Field on Ordering and Dynamics. *J. Chem. Theory Comput.* **2012**, *8*, 4807−4817.
(50) Wolf, M. G.; Hoefling, M.; Aponte-Santamaría, C.; Grubmüller, H.; Groenhof, G. g_membed: Efficient Insertion of a Membrane Protein into an Equilibrated Lipid Bilayer with Minimal Perturbation. *J. Comput. Chem.* **2010**, *31*, 2169−2174.
(51) Hess, B. P-LINCS: A Parallel Linear Constraint Solver for Molecular Simulation. *J. Chem. Theory Comput.* **2008**, *4*, 116−122.
(52) Hess, B.; Kutzner, C.; van der Spoel, D.; Lindahl, E. GROMACS 4: Algorithms for Highly Efficient, Load-Balanced, and Scalable Molecular Simulation. *J. Chem. Theory Comput.* **2008**, *4*, 435−447.
(53) May, S. Theories on Structural Perturbations of Lipid Bilayers. *Curr. Opin. Colloid Interface Sci.* **2000**, *5*, 244−249.
(54) Tatur, S.; Maccarini, M.; Barker, R.; Nelson, A.; Fragneto, G. Effect of Functionalized Gold Nanoparticles on Floating Lipid Bilayers. *Langmuir* **2013**, *29*, 6606−6614.
(55) Böckmann, R. A.; Hac, A.; Heimburg, T.; Grubmüller, H. Effect of Sodium Chloride on a Lipid Bilayer. *Biophys. J.* **2003**, *85*, 1647−1655.
(56) Harroun, T. A.; Heller, W. T.; Weiss, T. M.; Yang, L.; Huang, H. W. Experimental Evidence for Hydrophobic Matching and Membrane-Mediated Interactions in Lipid Bilayers Containing Gramicidin. *Biophys. J.* **1999**, *76*, 937−945.
(57) Kim, T.; Lee, K. I.; Morris, P.; Pastor, R. W.; Andersen, O. S.; Im, W. Influence of Hydrophobic Mismatch on Structures and Dynamics of Gramicidin A and Lipid Bilayers. *Biophys. J.* **2012**, *102*, 1551−1560.
(58) Andersen, O. S.; Koeppe, R. E. Bilayer Thickness and Membrane Protein Function: an Energetic Perspective. *Annu. Rev. Biophys. Biomol. Struct.* **2007**, *36*, 107−130.
(59) Sparr, E.; Ash, W. L.; Nazarov, P. V.; Rijkers, D. T. S.; Hemminga, M. A.; Tieleman, D. P.; Killian, J. A. Self-Association of Transmembrane Alpha-Helices in Model Membranes: Importance of Helix Orientation and Role of Hydrophobic Mismatch. *J. Biol. Chem.* **2005**, *280*, 39324−39331.
(60) Yoo, J.; Cui, Q. Membrane-Mediated Protein-Protein Interactions and Connection to Elastic Models: a Coarse-Grained Simulation Analysis of Gramicidin A Association. *Biophys. J.* **2013**, *104*, 128−138.
(61) Mecke, A.; Lee, D.-K.; Ramamoorthy, A.; Orr, B. G.; Banaszak Holl, M. M. Membrane Thinning Due to Antimicrobial Peptide Binding: an Atomic Force Microscopy Study of MSI-78 in Lipid Bilayers. *Biophys. J.* **2005**, *89*, 4043−4050.
(62) Wang, B.; Zhang, L.; Bae, S. C.; Granick, S. Nanoparticle-Induced Surface Reconstruction of Phospholipid Membranes. *Proc. Natl. Acad. Sci. U.S.A.* **2008**, *105*, 18171−18175.
(63) Nagle, J. F.; Tristram-Nagle, S. Structure of Lipid Bilayers. *Biochim. Biophys. Acta* **2000**, *1469*, 159−195.
(64) Alwarawrah, M.; Dai, J.; Huang, J. A Molecular View of the Cholesterol Condensing Effect in DOPC Lipid Bilayers. *J. Phys. Chem. B* **2010**, *114*, 7516−7523.
(65) Vermeer, L. S.; de Groot, B. L.; Rat, V.; Milon, A.; Czaplicki, J. Acyl Chain Order Parameter Profiles in Phospholipid Bilayers: Computation from Molecular Dynamics Simulations and Comparison with 2H NMR Experiments. *Eur. Biophys. J.* **2007**, *36*, 919−931.
(66) Douliez, J.-P.; Ferrarini, A.; Dufourc, E.-J. On the Relationship Between C-C and C-D Order Parameters and Its Use for Studying the Conformation of Lipid Acyl Chains in Biomembranes. *J. Chem. Phys.* **1998**, *109*, 2513−2518.
(67) Mihailescu, M.; Vaswani, R. G.; Jardn-Valadez, E.; Castro-Romn, F.; Freites, J. A.; Worcester, D. L.; Chamberlin, A. R.; Tobias, D. J.; White, S. H. Acyl-Chain Methyl Distributions of Liquid-Ordered and -Disordered Membranes. *Biophys. J.* **2011**, *100*, 1455−1462.

(68) Grafmüller, A.; Shillcock, J.; Lipowsky, R. The Fusion of Membranes and Vesicles: Pathway and Energy Barriers from Dissipative Particle Dynamics. *Biophys. J.* **2009**, *96*, 2658−2675.
(69) Kawamoto, S.; Shinoda, W. Free Energy Analysis Along the Stalk Mechanism of Membrane Fusion. *Soft Matter* **2014**, *10*, 3048−3054.
(70) Stevens, M. J.; Hoh, J. H.; Woolf, T. B. Insights into the Molecular Mechanism of Membrane Fusion from Simulation: Evidence for the Association of Splayed Tails. *Phys. Rev. Lett.* **2003**, *91*, 188102.
(71) Chakraborty, H.; Tarafdar, P. K.; Bruno, M. J.; Sengupta, T.; Lentz, B. R. Activation Thermodynamics of Poly(ethylene glycol)-Mediated Model Membrane Fusion Support Mechanistic Models of Stalk and Pore Formation. *Biophys. J.* **2012**, *102*, 2751−2760.
(72) Tu, Y.; Lv, M.; Xiu, P.; Huynh, T.; Zhang, M.; Castelli, M.; Liu, Z.; Huang, Q.; Fan, C.; Fang, H.; et al. Destructive Extraction of Phospholipids from Escherichia Coli Membranes by Graphene Nanosheets. *Nat. Nanotechnol.* **2013**, *8*, 594−601.